Origin of the p -band replicas in the electronic structure of graphene grown on 4H -SiC(0001)

Editors' Suggestion

Origin of the π-band replicas in the electronic structure of graphene grown on 4*H*-SiC(0001)

C. M. Polley,[1,2] L. I. Johansson,[3] H. Fedderwitz,[1] T. Balasubramanian,[1] M. Leandersson,[1] J. Adell,[1] R. Yakimova,[3] and C. Jacobi[3,4]

[1]*MAX IV Laboratory, Lund University, 221 00 Lund, Sweden*

[2]*Department of Microtechnology and Nanoscience, Chalmers University of Technology, Quantum Device Laboratory, Göteborg, Sweden*

[3]*Department of Physics, Chemistry and Biology, Linköping University, SE-58183 Linköping, Sweden*

[4]*Physics and Materials Science Research Unit, University of Luxembourg, 162a, avenue de la Faïencerie, L-1511, Luxembourg*

(Received 21 November 2018; published 5 March 2019)

The calculated electronic band structure of graphene is relatively simple, with a Fermi surface consisting only of six Dirac cones in the first Brillouin zone—one at each $\bar{K}$. In contrast, angle-resolved photoemission measurements of graphene grown on SiC(0001) often show six satellite Dirac cones surrounding each primary Dirac cone. Recent studies have reported two further Dirac cones along the $\bar{\Gamma}$-$\bar{K}$ line, and argue that these are not photoelectron diffraction artifacts but real bands deriving from a modulation of the ionic potential in the graphene layer. Here we present measurements using linearly polarized synchrotron light which show all of these replicas as well as several additional ones. Using information obtained from dark corridor orientations and angular warping, we demonstrate that all but one of these additional features—including those previously assigned as real initial-state bands—are possible to explain by simple final-state photoelectron diffraction.

DOI: 10.1103/PhysRevB.99.115404

I. INTRODUCTION

Graphene, one layer of carbon atoms arranged in a honeycomb structure, has made a major impact on both fundamental and applied condensed-matter physics [1,2] due to a long list of impressive properties. In particular, the peculiar "Dirac cone" band structure of free-standing graphene, with linear energy-momentum dispersion close to the Fermi energy and a Dirac point at the Fermi energy, makes it attractive for the development of carbon based nanoelectronics. However free-standing graphene is impractical for device applications, and so a suitable substrate is needed. Large-scale epitaxial films with atomic layer defined termination have been grown on Si-terminated SiC substrates [3,4]. However the electronic structure of graphene is influenced by symmetry breaking when employing substrates whose lattice symmetry does not match that of graphene [5–7].

One example of substrate-induced effects is the presence of six replica Dirac cone satellites around each $\bar{K}$, observed already in early angle-resolved photoemission (ARPES) studies of graphene grown on SiC(0001) [5,6]. These replicas have the same relative separation and orientation as the rosette spots observed around the 1×1 SiC and graphene spots in low-energy electron-diffraction (LEED) patterns, and so were explained to have a similar origin, i.e., to originate from photoelectron diffraction.

Additional replicas were reported in more recent ARPES investigations of graphene on SiC. Nevius *et al.* observed three more replicas in a 1-monolayer (ML) sample [8] and attributed them to umklapp photoelectron scattering. Nakatsuji *et al.* observed two of these three replicas in 1-ML but not 2-ML graphene samples [9], while Huang *et al.* observed the same two replicas in both 1- and 3-ML graphene samples [10]. Both Nakatsuji and Huang attributed the replicas to a modulation of the ionic potential in the graphene layer(s) induced by the charge modulation of the carbon layer at the interface, i.e., the carbon buffer layer. This constitutes an "initial state" interpretation in which the features correspond to electronic bands as opposed to a "final state" artifact due to photoelectron diffraction. With ARPES it is typically very difficult to distinguish between the two cases. The only definitive observation is an avoided crossing (band gap) where replica bands intersect, which proves an initial-state effect. This is for example the case with graphene grown on Ir(111) [11], but to date such avoided crossings have never been observed for SiC graphene. However since energy resolution is always finite, failure to observe a gap does not prove that no gap exists.

Here we argue that this ambiguity about the origin of the replicas is still unresolved for graphene on SiC. With one inconclusive exception, all replicas can be fully explained with a combination of final-state photoelectron diffraction and subtle experimental effects relating to measurement geometry and sample homogeneity. Nakatsuji and Huang performed ARPES measurements with unpolarized He-I radiation, which results in constant energy surfaces with uniform intensity. Here we investigate monolayer and multilayer graphene samples using linearly polarized synchrotron radiation, which causes the Dirac cones to exhibit a "dark corridor" of reduced intensity [12]. Since the orientation of the dark corridor is different for each $\bar{K}$ in the first Brillouin zone, this reveals the parent Dirac cone for all but one of the π-band replicas.

II. EXPERIMENTAL METHODS

Graphene samples were sublimation grown [3,13] *ex situ* on *n*-type wafers of 4*H*-SiC(0001) purchased from SiCrystal. Samples with different numbers of graphene layers were

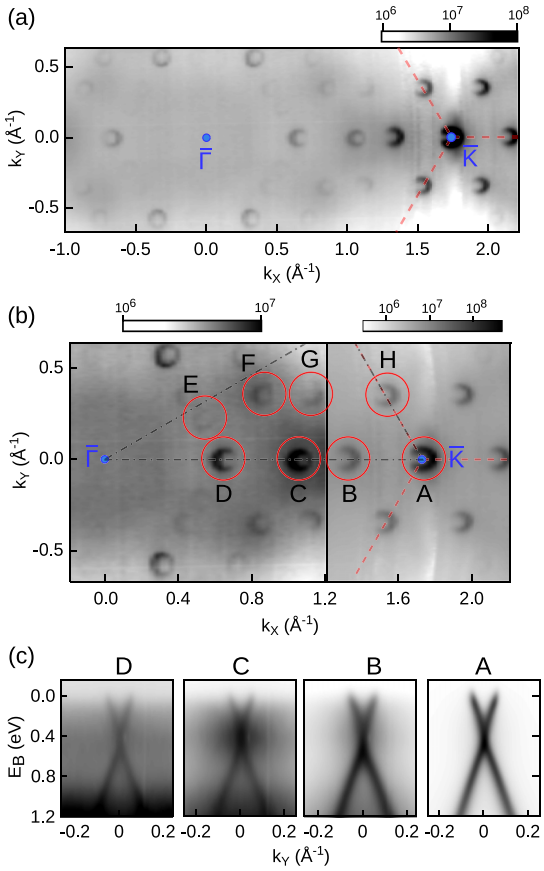

FIG. 1. (a) The Fermi surface of a 1-ML graphene sample grown on a 4*H*-SiC(0001) substrate using *p*-polarized 40-eV photons. (b) The same measurement presented with two different color scales in order to visualize all features. The positions of eight different Fermi pockets are highlighted within the $\bar{\Gamma}$-$\bar{K}$-$\bar{M}$ wedge. (c) (E, k_Y) cuts through four of the features, each showing identical Dirac-like dispersions.

obtained by varying the growth time or temperature. In sublimation growth of graphene on SiC(0001) an insulating carbon "buffer" layer is always formed first, with subsequent graphene layers growing over it. This buffer layer gives rise to a characteristic $6\sqrt{3} \times 6\sqrt{3}R30^\circ$ LEED pattern [3,14].

ARPES measurements were performed at beamline i4 at the MAX-IV Laboratory, which is equipped with a spherical grating monochromator and a PHOIBOS 100 hemispherical electron analyzer from SPECS. Photon energies of 36 and 40 eV were chosen to maximize the intensity of the replica bands. Each ARPES spectrum was collected perpendicular to the $\bar{\Gamma}$-$\bar{K}$ direction of the Brillouin zone (BZ) of graphene, in steps of 0.5° along the $\bar{\Gamma}$-$\bar{K}$ direction. To accommodate the large dynamic range without overloading the photoelectron detector, the beamline flux was manually adjusted while measuring. For this reason our data provide a qualitative rather than quantitative estimate of the intensity differences between features. Some data sets were collected with the sample at a temperature of around 100 K and some with the sample at room temperature. A clean Ta foil in electrical contact with the sample was used to reference the Fermi-level position.

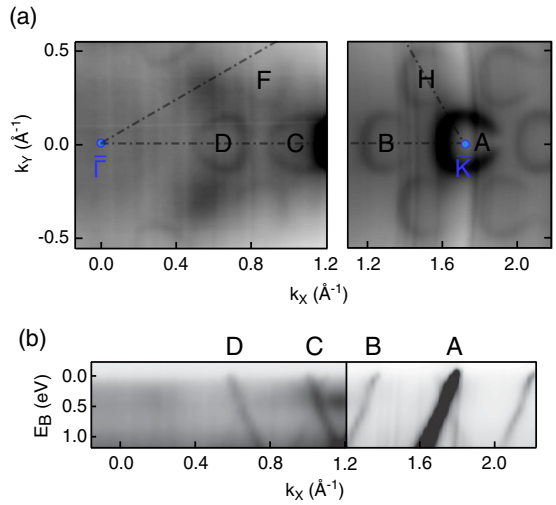

FIG. 2. (a) The measurement data from Fig. 1, here visualized as an $E_B = 1.3$ eV constant energy surface to emphasize the trigonal warping of the Dirac cones. (b) An (E, k_X) cut through $k_Y = 0$, from which the reversal of the dark corridor orientations is clear for the Dirac cones A and B compared to C and D.

III. RESULTS AND DISCUSSION

The Fermi surface of a 1-ML graphene sample grown on SiC(0001) is shown in Fig. 1(a). The image shows the main Dirac cone at $\bar{K}$ ($k_X = 1.7$ Å^{-1}), surrounded by six replica cones forming a hexagonal rosette pattern. Several additional, weaker features are also present. Some of these are more than 1000 times less intense than the primary Dirac cones at $\bar{K}$, and so only barely resolvable. In order to visualize those more clearly, Fig. 1(b) replots part of this data set with a dual, logarithmic color scale. Here the additional replicas are clearly visible, along with the orientation of the dark corridor in each replica. We have labeled as A–H the eight unique features within the $\bar{\Gamma}$-$\bar{K}$-$\bar{M}$ wedge. None of these bands show any evidence of avoided crossings ("minigaps") where they intersect. This is consistent with previous studies of graphene on SiC, but it is also not conclusive. It may simply mean that the gaps are too small to resolve experimentally

Features C and D were observed previously by Nakatsuji and Huang, while Nevius observed features C,D, and F. Figure 1(c) shows high-resolution (E, k_Y) cuts through each of the four features found on the $\bar{\Gamma}$-$\bar{K}$ line. Along this direction the intensity is symmetric in both branches of the π band. It is clear that all four of these features have identical dispersions, in agreement with earlier observations [9,10].

Off the $\bar{\Gamma}$-$\bar{K}$ line, three more replicas can be found. These are labeled E–G in Fig. 1(b). Careful inspection reveals that the symmetry of features C–G does not match that of features A, B, and H. This is apparent in the orientation of the dark corridor, but also manifests in the orientation of the trigonal warping at higher binding energies. Figure 2(a) illustrates a reversal in the warping orientation for features C, D, and F compared with features A, B, and H. Figure 2(b) presents an (E, k_X) cuts at $k_Y = 0$ in order to highlight the differing dark corridor orientation of features A–D. Here it is clear that the more intense branch of the π bands reverses for C

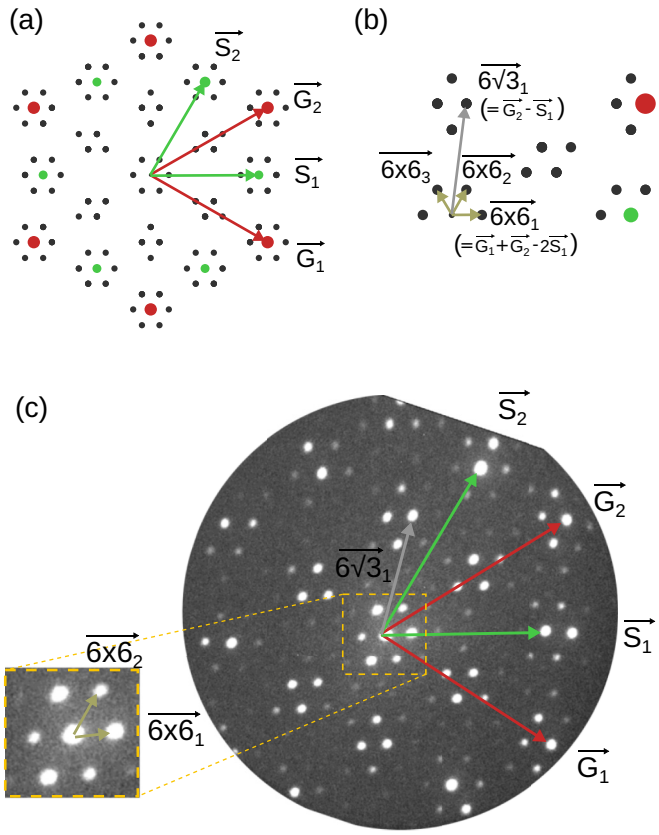

FIG. 3. (a),(b) Schematic depiction of the characteristic LEED pattern from sublimation grown graphene on 4*H*-SiC(0001). Scattering vectors are shown corresponding to the graphene layer ($\vec{G}$) and the SiC layer ($\vec{S}$), as well as selected vectors from the $6\sqrt{3}$ and 6×6 superlattices. (c) A μ-LEED pattern ($E = 45$ eV, 5-μm probing area) collected from a SiC(0001) sample prepared to have "zero monolayer" graphene coverage. The image was collected as part of an earlier study [15].

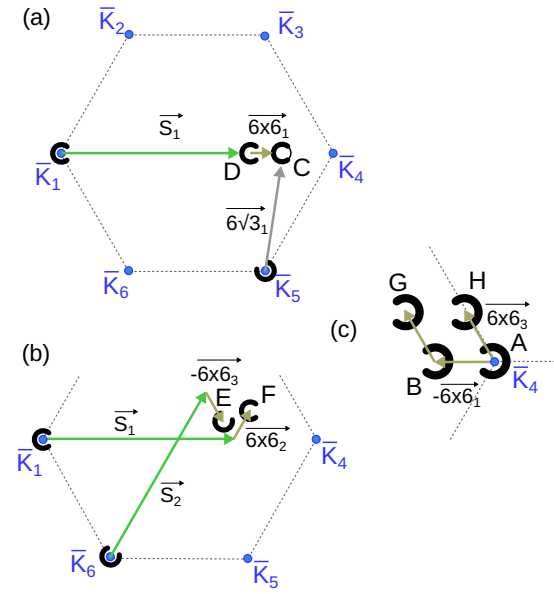

FIG. 4. Examples of scattering processes which can scatter photoelectrons from one of the primary Dirac cones at $\bar{K}$ to the locations of replica features B–H. While scattering processes are shown as vector sums, the buffer layer reconstruction makes all of these possible as one-step scattering events.

and D compared to A and B. If these replicas have originated from photoelectron diffraction, the dark corridor and warping orientation can be used to uniquely determine which $\bar{K}$ point each feature has scattered from.

A. Available scattering vectors

In the simplest possible picture, two sets of scattering vectors are available: the hexagonal SiC(0001) substrate ($a = 3.08$ Å) offers vectors S_1 and S_2 while the graphene ($a = 2.46$ Å) offers vectors G_1 and G_2, rotated by 30° with respect to the SiC lattice [Fig. 3(a)]. In reality the situation is more complicated. As the precursor to graphene formation, a carbon-rich buffer layer is formed on the SiC(0001), with a complicated reconstruction consisting of $6\sqrt{3}R30°$, 6×6, and 5×5 periodicities [14]. These periodicities are real in the sense that scanning tunneling microscopy can directly observe them as modulations of the electronic density of states, and photoelectrons can scatter from them as a one-step process. All linear combinations of these reciprocal-lattice vectors represent possible scattering events, but in practice only a limited subset are relevant for scattering. This is clear from LEED images of SiC graphene, which are typically dominated by spots from the SiC and graphene 1×1 lattice, 6×6 satellites around these, and four additional intense spots between the zeroth- and first-order graphene spots. This is depicted in Figs. 3(a) and 3(b). For two of these scattering vectors ($\overrightarrow{6\sqrt{3}_1}$ and $\overrightarrow{6 \times 6_1}$) we show also how they can be constructed from SiC and graphene basis vectors. In Fig. 3(c) we show a micro-LEED pattern recorded from a different SiC(0001) sample prepared with only the carbon buffer layer [15], i.e., "zero monolayer" graphene. The reciprocal-lattice vectors discussed above can be clearly seen.

Returning to the photoemission measurements, after the primary Dirac cone at $\bar{K}$ (labeled in Fig. 1 as feature A) the next most intense features in the $\bar{\Gamma}$-$\bar{K}$-$\bar{M}$ wedge are the nearby features B and H. These satellite Dirac cones are relatively intense and thus commonly observed in ARPES experiments [7,10]. They have the same relative separation and orientation as the 6×6 satellite spots observed in LEED images [3,14]. This correspondence suggests that the origin of features B and H could be scattering of photoelectrons emerging from the nearby Dirac cone, by the vectors $-\overrightarrow{6 \times 6_1}$ and $\overrightarrow{6 \times 6_3}$. Further support for this suggestion is found by examining the orientation of both the dark corridor at $E_B = E_F$ in Fig. 1 and the trigonal warping at $E_B = 1.3$ eV in Fig. 2. Both properties match that of the parent Dirac cone at $\bar{K}$.

If we assume that the trigonal warping and dark corridor orientation are preserved during photoelectron diffraction, the remaining five replicas cannot originate from the same $\bar{K}$ point. The features we have labeled C and D have also been observed in at least two previous studies [9,10], and have been ascribed to an initial-state effect, i.e., new electronic bands owing to the superperiodic modulation of the graphene potential [10]. However in Fig. 4(a) we highlight that simple scattering processes can also produce these features as a final-state photoelectron diffraction effect. A process involving $\vec{S}_1$

can scatter photoelectrons from $\bar{K}_1$ to the position of feature D, while a vector such as $(\vec{S_1} + \overrightarrow{6 \times 6_1})$ can scatter from $\bar{K}_1$ to the position of feature C. Photoelectron scattering by these processes would be consistent with the experimentally observed replica symmetry. Previous studies of these replicas employed unpolarized radiation from a He lamp [9,10], which eliminates the dark corridor and hence conceals this clue about the possible origin of the replicas.

In fact there are many possible scattering paths that could contribute to these features, not all of which are shown here. In the case of feature C this includes scattering not just from $\bar{K}_1$ but also $\bar{K}_3$ and $\bar{K}_5$ (for example by $\overrightarrow{6\sqrt{3}_1}$ as shown). This may be the reason that the dark corridor of feature C is less pronounced than that of feature D: weak contributions to replica C from $\bar{K}_3$ and $\bar{K}_5$ would fill in some of the missing intensity in the dark corridor. However we emphasize again that while many scattering processes are in principle possible, experimental LEED patterns leave no doubt that these processes are not all equally likely.

Feature E has not been discussed in the literature, while Feature F has been seen in only one prior study [8]. This is presumably owing to their very low intensity. Based on their location and the orientation of their dark corridors, both can be explained by a photoelectron diffraction process, as illustrated in Fig. 4(b). In this interpretation, feature E is a replica from $\bar{K}_6$ while feature F is a replica from $\bar{K}_1$.

The final feature, G, has also has not been discussed previously, and is less straightforward. The location in the Brillouin zone suggests that it originates from $\bar{K}_4$ by way of a scattering vector which is the sum of two $\overrightarrow{6 \times 6}$ vectors, as shown in Fig. 4(c). However, careful inspection of the experimentally observed dark corridor orientation rather suggests that it originates from $\bar{K}_5$. This apparent contradiction is difficult to explain, since we cannot identify any combination of scattering vectors that can link feature G to $\bar{K}_5$. The intensity of this feature is too low to resolve the trigonal warping at higher binding energies.

Since photoelectron diffraction is closely related to LEED, it is instructive to examine the relative intensities of different LEED spots. The relative intensities seen in Fig. 3(c) are qualitatively similar for energies down to at least 32 eV. It is clear that certain electron-scattering combinations are more likely to occur than others. For example, in Fig. 3(c) the 6×6 satellite spots surrounding the $\vec{S_1}$ spot are strongly modulated, with the highest intensity corresponding to forward scattering (i.e., $\vec{S_1} + \overrightarrow{6 \times 6_1}$) and the weakest to backscattering (i.e., $\vec{S_1}$-$\overrightarrow{6 \times 6_1}$). This matches well with the replicas in the ARPES measurements: Of six possible $(\vec{S} + \overrightarrow{6 \times 6})$-type replicas, the directly forward scattering combination is the most intense (replica C), followed by the partially forward scattering combinations (replica F) and then the partially backscattered combinations (replica E). No replica was observed corresponding to the directly backscattering combination.

B. >1-ML graphene

In an earlier study, Nakatsuji *et al.* reported [9] that the two replicas labeled C and D exist in 1-ML graphene but vanish in 2-ML graphene. A subsequent study by Huang *et al.* reported [10] that these replicas exist in both 1- and 3-ML graphene samples. To clarify this apparent contradiction, we have also investigated samples grown to give multilayer graphene coverage. The Fermi surface obtained from one of those samples is shown in Fig. 5(a). A comparison with Fig. 1(b) shows that all features from the 1-ML sample persist. Replicas C and D are very clearly present, while features E–G are just barely observable [clearest in the lower half of Fig. 5(a)].

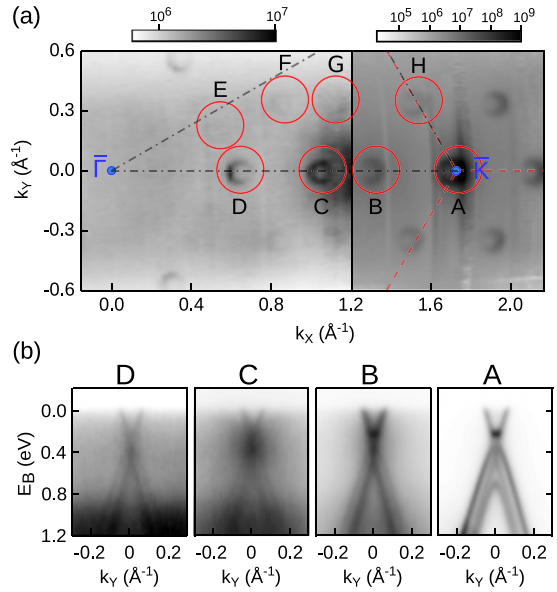

FIG. 5. (a) The Fermi surface recorded from a multilayer graphene sample grown on a 4*H*-SiC(0001) substrate using *p*-polarized 40-eV photons. The locations of the eight features in the 1-ML sample are highlighted. (b) (E, k_Y) cuts through features A–D. While the number and dispersion of the bands are the same for each feature, the relative intensities of the inner and outer bands vary strongly.

The π-band structure for features A–D, recorded perpendicular to $\bar{\Gamma}$-$\bar{K}$, is shown in Fig. 5(b). A careful inspection of the primary Dirac cone (A) shows that it is composed of one linear π band as for monolayer graphene and two quadratic dispersing π bands as for *AB* stacked bilayer graphene. This dispersion is essentially identical to that reported by Huang *et al.* [10], and was interpreted as 3-ML coverage. Indeed, the calculated band structure for Bernal stacked (*ABA*) free-standing 3-ML graphene [16,17] looks very similar to this. Nonetheless, in the absence of low-energy electron microscopy measurements it is not possible to conclude whether our spectra in Fig. 5 correspond to homogeneous 3-ML coverage or instead an averaging of 1- and 2-ML domains. We expect our samples, furnace grown *ex situ* in an Ar ambient, to show larger homogeneity in the graphene coverage than samples grown *in situ* by thermal annealing [3,4,18,19]. The previous studies by Nakatsuji and Huang used *in situ* grown samples, and so are also subject to this uncertainty regarding the coverage.

Comparing the π-band structure of the primary Dirac cone with that of replicas B–D [Fig. 5(b)] shows that while all four features have the same number of bands and band dispersion,

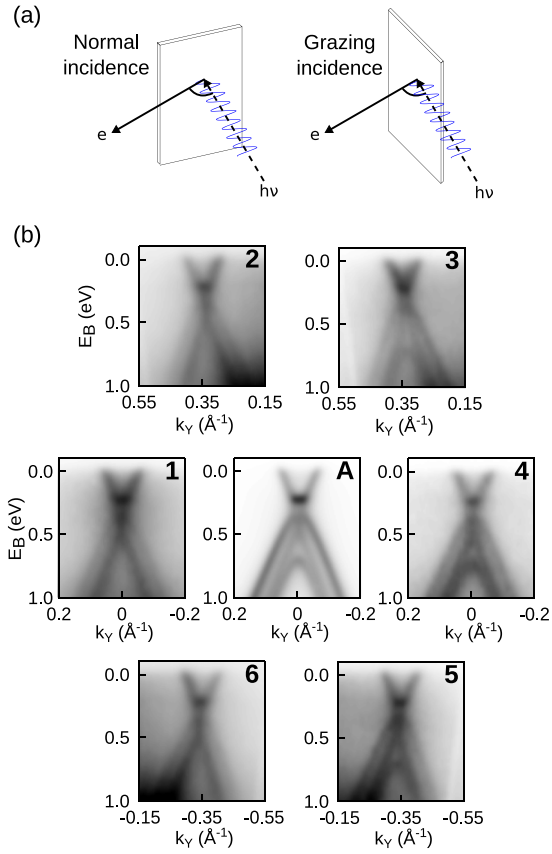

FIG. 6. (a) Schematic of the polarization geometry. As the sample is rotated during the course of an ARPES measurement, the electric-field vector of *p*-polarized light evolves from being in the sample plane at normal incidence, to being out of plane at grazing incidence. (b) (E, k_Y) cuts of the primary Dirac cone at $\bar{K}_4$ and the $\overrightarrow{6 \times 6}$ satellites around it. While all six satellites should have identical intensity patterns, here it is clear that the relative intensity of the inner and outer bands depends on the k_X location of the feature, i.e., the polar rotation of the sample.

the relative intensity of each band differs across the replicas. For the main Dirac cone (A) the quadratic dispersing π bands are dominant, while for the replicas the linear π band dominates. The same observation was made by Huang *et al.* [10], and offered as a key argument in support of an initial-state origin for these replicas. Indeed, it is difficult to explain how a scattering process could result in such pronounced differences in relative intensities.

Here we wish to point out an alternative explanation. An experimental detail of all published studies to date is the need to rotate the sample in order to examine different regions in the surface Brillouin zone. Since the light source and electron analyzer remain fixed, the polarization geometry is continuously changing. For the 40-eV light used in Fig. 5 the sample was rotated by 22° between measuring features D and A. In our case the electric-field vector lies purely out of plane of the sample surface when at grazing incidence, and purely in plane at normal incidence. This is depicted in Fig. 6(a). As the sample normal is rotated towards the light source, the in-plane and out-of-plane projections change. This effect is lessened but still present when using a helium discharge lamp with randomized polarization. While the out-of-plane projection of the electric-field vector is only 50% at grazing incidence, the lower photon energy (21.2 eV) demands much larger changes in rotation angle. Several authors have shown that the intensity distributions in the π bands of single- and multilayer graphene are strongly affected by changes in the polarization geometry [12,20,21]. Hence, an alternative explanation for the differing intensity patterns in Fig. 5(b) may simply be the differing polarization geometry when measuring them.

This possibility can be supported by careful examination of all six of the replicas in the immediate vicinity of feature A at $\bar{K}_4$ [Fig. 6(b)]. In the absence of polarization effects, all six satellites should have identical intensity patterns regardless of whether they originate from initial-state bands or from photoelectron diffraction. A comparison of replicas 1 and 4 clearly shows that this is not the case. The hexagonal arrangement of replicas provides an opportunity to compare features measured at the same rotation angle [pairs (2,6) and (3,5)]. Within these pairs the intensity pattern is very similar, supporting the possibility that the unusual variation in intensity distribution may simply be an experimental artifact relating to a varying polarization geometry.

The preceding discussion about intensity variations may call into question the validity of our use of the dark corridor orientation when attempting to establish the origin of the replica peaks. This is trivially addressed for all but two of the replicas by noting that the trigonal warping is visible, and it corroborates the dark corridor orientation [Fig. 2(a)]. It then seems reasonable to assume that replicas E and G follow this trend and have preserved their orientation.

Finally, there is one additional experimental detail which should be taken into consideration. When rotating the sample away from normal incidence, the size of the light spot footprint on the sample increases. In the likely event that the sample surface is not perfectly located at the manipulator center of rotation, the position of the light spot on the sample will also change. Both of these observations are relevant if the sample is not perfectly uniform but instead contains a mixture of 1- and >1-ML graphene domains. This has the potential to cause the kind of variations in relative intensity shown in Figs. 5 and 6.

IV. CONCLUSIONS

The π-band replicas observed in ARPES studies of graphene grown on SiC(0001) could originate from either final-state photoelectron diffraction or initial-state band-structure modifications due to charge modulation by the carbon buffer layer. In the absence of obvious band crossings or anticrossings, it is very difficult to decide on the origin of replicas using only ARPES. Two earlier ARPES studies have argued firmly in favor of an initial-state origin of the π-band replicas in SiC graphene [9,10]. Here we have presented measurements using linearly polarized synchrotron radiation, in which we observe numerous replica bands and their symmetry of all replicas. We have shown that an interpretation in terms of final-state diffraction remains sufficient to account

for the location and symmetry of all π-band replicas, with the possible exception of a previously unobserved replica (G). These measurements do not constitute proof of a final-state origin, but rather show that, in contrast to earlier studies, the situation remains undecided. Arguments based on differing intensity distributions are not conclusive without properly controlling for both the polarization geometry and sample homogeneity. In this regard, future experiments repeating these measurements with an apparatus that does not require moving the sample with respect to the light spot may prove illuminating.

ACKNOWLEDGMENTS

We thank J. Osiecki for creating the data analysis software used here. This work was made possible through support from the Knut and Alice Wallenberg Foundation and the Swedish Research Council.

[1] A. K. Geim and K. S. Novoselov, The rise of graphene, Nat. Mater. **6**, 183 (2007).

[2] A. H. Neto, F. Guinea, N. M. R. Peres, K. S. Novoselov, A. K. Geim, The electronic properties of graphene, Rev. Mod. Phys. **81**, 109 (2009).

[3] C. Virojanadara, M. Syväjarvi, R. Yakimova, L. I. Johansson, A. A. Zakharov, and T. Balasubramanian, Homogeneous large-area graphene layer growth on 6H-SiC(0001), Phys. Rev. B **78**, 245403 (2008).

[4] K. V. Emtsev, A. Bostwick, K. Horn, J. Jobst, G. L. Kelloff, L. Ley, J. L. McChesney, T. Ohta, S. A. Reshanov, J. Röhrl, E. Rotenberg, A. K. Schmid, D. Waldmann, H. B. Weber, and T. Seyller, Towards wafer-size graphene layers by atmospheric pressure graphitization of silicon carbide, Nat. Mater. **8**, 203 (2009).

[5] A. Bostwick, T. Ohta, J. L. McChesney, K. V. Emtsev, T. Seyller, K. Horn, and E. Rotenberg, Symmetry breaking in few layer graphene films, New J. Phys **9**, 385 (2007).

[6] A. Bostwick, T. Ohta, T. Seyller, K. Horn, and E. Rotenberg, Quasiparticle dynamics in graphene, Nat. Phys. **3**, 36 (2007).

[7] E. Rotenberg and A. Bostwick, Superlattice effects in graphene on SiC(0001) and Ir(111) probed by ARPES, Synth. Met. **210**, 85 (2015).

[8] M. S. Nevius, M. Conrad, F. Wang, A. Celis, M. N. Nair, A. Taleb-Ibrahimi, A. Tejeda, and E. H. Conrad, Semiconducting Graphene from Highly Ordered Substrate Interactions, Phys. Rev. Lett. **115**, 136802 (2015).

[9] K. Nakatsuji, Y. Shibata, R. Niikura, F. Komori, K. Morita, and S. Tanaka, Shape, width, and replicas of π bands of single-layer graphene grown on Si terminated vicinal SiC(0001), Phys. Rev. B **82**, 045428 (2010).

[10] L. Huang, Y. Wu, M. T. Hershberger, D. Mou, B. Schrunk, M. C. Tringides, M. Hupalo, and A. Kaminksi, Effects of moiré lattice structure on electronic properties of graphene, Phys. Rev. B **96**, 035411 (2017).

[11] I. Pletikosić, M. Kralk, P. Pervan, R. Brako, J. Coraux, A. T. N'Diaye, C. Busse, and T. Michely, Dirac Cones and Minigaps for Graphene on Ir(111), Phys. Rev. Lett. **102**, 056808 (2009).

[12] I. Gierz, J. Henk, H. Höchst, C. R. Ast, and K. Kern, Illuminating the dark corridor in graphene: Polarization dependence of angle-resolved photoemission spectroscopy on graphene, Phys. Rev. B **83**, 121408(R) (2011).

[13] A. Tzalenchuk, S. Lara-Avila, A. Kalaboukhov, S. Paolillo, M. Syväjärvi, R. Yakimova, O. Kazakova, T. J. B. M. Janssen, V. Fal'ko, and S. Kubatkin, Nat. Nanotechnol. **5**, 186 (2010).

[14] C. Riedl, U. Starke, J. Bernhardt, M. Franke, and K. Heinz, Structural properties of the graphene-SiC(0001) interface as a key for the preparation of homogeneous large-terrace graphene surfaces, Phys. Rev. B **76**, 245406 (2007).

[15] C. Virojanadara, A. A. Zakharov, S. Watcharinyanon, R. Yakimova, and L. I. Johansson, A low-energy electron microscopy and x-ray photo-emission electron microscopy study of Li intercalated into graphene on SiC(0001), New J. Phys. **12**, 125015 (2010).

[16] C. Coletti, S. Forti, A. Principi, K. V. Emtsev, A. A. Zakharov, K. M. Daniels, B. K. Daas, M. V. S. Chandrashekhar, T. Ouisse, D. Chaussende, A. H. MacDonald, M. Polini, and U. Starke, Revealing the electronic band structure of trilayer graphene on SiC: An angle-resolved photoemission study, Phys. Rev. B **88**, 155439 (2013).

[17] C. Bao, W. Yao, E. Wang, C. Chen, J. Avila, M. C. Asensio, and S. Zhou, Stacking-Dependent Electronic Structure of Trilayer Graphene Resolved by Nanospot Angle-Resolved Photoemission Spectroscopy, Nano Lett. **17**, 1564 (2017).

[18] T. Ohta, F. El Gabaly, A. Bostwick, J. L. McChesney, K. V. Emtsev, A. K. Schmid, T. Seyller, K. Horn, and E. Rotenberg, Morphology of graphene thin film growth on SiC(0001), New J. Phys **10**, 023034 (2008).

[19] C. Virojanadara, R. Yakimova, A. A. Zakharov, and L. I. Johansson, Large homogeneous mono-/bi-layer graphene on 6H-SiC(0001) and buffer layer elimination, J. Phys. D: Appl. Phys. **43**, 374010 (2010).

[20] C. Hwang, C.-H. Park, D. A. Siegel, A. V. Fedorov, S. G. Louie, and A. Lanzara, Direct measurement of quantum phases in graphene via photoemission spectroscopy, Phys. Rev. B **84**, 125422 (2011).

[21] Y. Liu, G. Bian, T. Miller, and T.-C. Chiang, Visualizing Electronic Chirality and Berry Phases in Graphene Systems Using Photoemission with Circularly Polarized Light, Phys. Rev. Lett. **107**, 166803 (2011).